



HAL
open science

Ambient moisture influence on the secondary relaxations of epoxy-amine networks with different crosslink densities

Carolina Helena Franzon, Aurélien Roggero, Sébastien Pruvost, Jean-François Gérard

► To cite this version:

Carolina Helena Franzon, Aurélien Roggero, Sébastien Pruvost, Jean-François Gérard. Ambient moisture influence on the secondary relaxations of epoxy-amine networks with different crosslink densities. *Polymer*, 2024, 315 (17), pp.127750. 10.1016/j.polymer.2024.127750 . hal-04837497

HAL Id: hal-04837497

<https://hal.science/hal-04837497v1>

Submitted on 13 Dec 2024

HAL is a multi-disciplinary open access archive for the deposit and dissemination of scientific research documents, whether they are published or not. The documents may come from teaching and research institutions in France or abroad, or from public or private research centers.

L'archive ouverte pluridisciplinaire **HAL**, est destinée au dépôt et à la diffusion de documents scientifiques de niveau recherche, publiés ou non, émanant des établissements d'enseignement et de recherche français ou étrangers, des laboratoires publics ou privés.

Ambient moisture influence on the secondary relaxations of epoxy-amine networks with different crosslink densities

Carolina Helena Franzon^a, Aurélien Roggero^{a,*}, Sébastien Pruvost^a, Jean-François Gérard^a

^aUniversité Claude Bernard Lyon 1, INSA Lyon, Université Jean Monnet, CNRS UMR 5223, Ingénierie des Matériaux Polymères, F-69621, Villeurbanne, France

Abstract

The molecular mobility of polyepoxy networks synthesized from diglycidyl ether of bisphenol-A (DGEBA) and cured with aliphatic diamines featuring varying polypropylene glycol (PPG) backbone lengths was investigated. The influence of ambient storage conditions, notably absorbed moisture, in conjunction with the network crosslink density on physical properties, was explored by using multiple techniques, including differential scanning calorimetry, dielectric and mechanical spectroscopies. In addition to known effects on glass transition and its dynamic manifestations, significant effects on secondary relaxation modes were observed, further highlighting the importance of controlling initial sample conditions when conducting molecular mobility studies. A bimodal β -relaxation was observed in the presence of absorbed moisture as a result of an additional water-related mode, β_2 , ascribed to hydroxyether groups interacting with water.

Keywords: polymer network, crosslink density, water interaction, molecular relaxations, dynamic mechanical analysis, dielectric spectroscopy

1. Introduction

Numerous studies have been devoted to the understanding of the molecular motions responsible for epoxy networks' relaxations [1–13]. The dependence of the main structural relaxation, α , associated with the glass transition, on network architecture is well understood and has been extensively studied [1, 2]. Conversely, a comparable level of comprehension concerning epoxy secondary relaxations is yet to be achieved in order to establish structure-properties relationships in the glassy state. Various techniques, including torsion pendulum [3–6], dynamical mechanical analysis (DMA) [7–9, 14], broadband dielectric spectroscopy (BDS) [11], and solid-state NMR [9, 10] were used and combined with strategies of controlled changes in chemical structure [3–5, 7–10, 14], curing degree [11] and stoichiometry [3, 4, 6, 14], aiming to understand the motional processes involved in secondary relaxation modes.

Three secondary modes were identified in both mechanical and dielectric relaxation spectra of polyepoxy networks, *i.e.* γ , β , and ω . The lower temperature γ process occurring below -100 °C at 1 Hz, has been commonly ascribed to the motion of polymethylene sequences within the network [3, 5, 8, 15]. The minimum number of consecutive CH₂ units required to induce the γ motions depends on the flexibility of immediate neighboring segments [3, 8].

The main secondary process, β , is present in all epoxy-amine networks irrespective of the curing agent and network structure. The contribution from the hydroxyether unit, originating from

the epoxy-amine curing reaction, has been demonstrated in numerous studies [3–6, 9, 10]. Contributions of diphenylpropane unit [6, 16, 17] and phenyl ring flips [8] to the mode were also proposed.

Moreover, an additional contribution to the high-temperature side of the mode is often observed, characterized by an increase in both the overall amplitude and width of the loss peak [3, 4, 17, 18], and depending on the system, it can be seen as a shoulder [7–9, 14, 19–22]. The amplitude and extent of this contribution were found to be closely related to crosslink density [3, 8, 9, 14, 16, 21–23], and interpretations in terms of coupling of the motion processes involved in high crosslink density networks were proposed [8, 9].

An intermediary relaxation mode, referred to ω -relaxation, is often observed between the β and α modes in epoxy-amine networks. This relaxation has been controversially discussed in literature. The mode has been reported as being highly sensitive to water [24–27], and in some cases, observed only in the presence of adsorbed water [27]. Some authors ascribed it to motions in lower crosslink density regions, implying the existence of heterogeneities in the network [4, 23, 28]. However, epoxy-amine networks can be homogeneous when an appropriate curing profile is selected to obtain fully crosslinked stoichiometric networks [29]. Other authors proposed that the mode would arise from conformational rearrangements following water absorption [30]. The sensitivity of the γ and β modes to water sorption, especially their increase in amplitude, has also been reported [20, 24, 26, 31].

In the vast majority of these mobility studies, the initial state of the network with regards to moisture content is not controlled. This is important as epoxy-amine networks are able to

*Corresponding author

Email address: aurelien.roggero@insa-lyon.fr (Aurélien Roggero)

absorb moisture leading to decrease in T_g in the order of 10 to 20 °C per weight percent of absorbed water [32, 33]. Although it is a well-controlled parameter in sorption studies, the influence of water on molecular mobility is often studied separately from structural architecture modifications [24, 31, 34].

The aim of this work is to correlate the effects of chemical structure and absorbed water on the molecular mobility of three aliphatic amine-based polyepoxy networks with different crosslink densities, by performing two consecutive heating runs in differential scanning calorimetry, dielectric and mechanical spectroscopies. The samples are equilibrated with ambient moisture prior to the first run and are dry during the second.

2. Experimental

2.1. Materials

The epoxy prepolymer used was diglycidyl ether of bisphenol-A (DGEBA) (Araldite® LY 556 from Huntsman). The amine curing agents used were a series of poly(propylene glycol) bis(2-aminopropyl ether), also known as Jeffamines. Different molar masses were considered, *i.e.* D230 ($\overline{M}_n = 240 \text{ g} \cdot \text{mol}^{-1}$) (Abr), D400 ($\overline{M}_n = 460 \text{ g} \cdot \text{mol}^{-1}$) (Huntsman), and D2000 ($\overline{M}_n = 2,056 \text{ g} \cdot \text{mol}^{-1}$) (Huntsman). The chemical structures of the prepolymers are represented in Table 1.

Three networks of different crosslink densities were obtained from the copolymerization of DGEBA and Jeffamines at amino-hydrogen-to-epoxy equal to 1, denoted as DGEBA/D230 (32.1 phr), DGEBA/D400 (61.5 phr), and DGEBA/D2000 (274.9 phr). The networks are represented in Figure 1, together with the theoretical average molar mass between crosslinks, \overline{M}_c , obtained from Bells's method [35]:

$$\overline{M}_c = \frac{2 M_{\text{epoxy}} + M_{\text{amine}}}{3} \quad (1)$$

where M_{epoxy} and M_{amine} are the molar masses of the DGEBA and amine prepolymers, respectively (values in Table 1). Bell's equation assumes a perfect network where all amino-hydrogens reacted with epoxide rings to form trifunctional crosslink junctions, consisting of one diamine and two diepoxy moieties. The stoichiometric networks here studied, synthesized under adequate curing protocol, should represent the best scenario to approach ideal networks.

2.2. Preparation of polyepoxy samples

DGEBA was pretreated at 80 °C under vacuum for 5 to 10 h to degas and remove absorbed moisture that could evaporate and form bubbles during curing. Then, the prepolymer was stored in an oven at a constant temperature of 50 °C. The Jeffamines were stored at 15 °C without pretreatment. The epoxy prepolymer and amine hardener were weighed and subjected to three consecutive mixing cycles of 10 minutes in a planetary mixer (Hauschild SpeedMixer®) under a vacuum of 30 mbar and a maximum speed of 2,000 rpm. The DGEBA/Jeffamine mixtures were carefully poured onto a steel plate coated with PTFE adhesive film and covered with an identical plate, spaced by 300 µm silicone film with maximum thickness variation of

less than ±5 %. The mold assembly was maintained during curing by homogeneously distributed clamps. The curing was performed in an oven at 80 °C for 2 h, 125 °C for 3 h, and 200 °C for 1 h, with a prior step at 45 °C for 1 h in the case of DGEBA/D230 network. After curing, the samples were removed from the mold at ambient temperature and stored under ambient conditions. The samples were obtained in the form of 300 µm-thick transparent films exhibiting less than ±10 % thickness variation. The three films obtained were used to perform all the subsequent analyses.

2.3. Thermogravimetric water uptake

Samples cut from the synthesized films, weighing approximately 250 mg, were dried at 90 °C under vacuum for approximately 20 hours. The samples were immediately weighed after removal from the oven and stored under ambient conditions. Then, they were periodically weighed with a 0.01 mg readability until equilibration was achieved.

2.4. Differential scanning calorimetry (DSC)

Differential scanning calorimetry measurements were carried out with a DSC 3 apparatus (Mettler Toledo). Small pieces of the obtained films were cut out to a total mass of approximately 10 mg and placed in an aluminium pan. Hermetic and non-hermetic pans were used to respectively limit or favour the desorption of absorbed water.

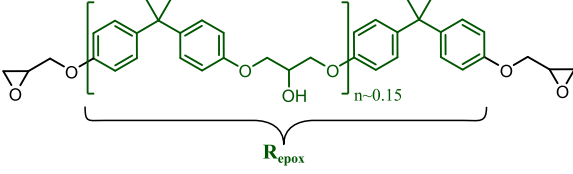
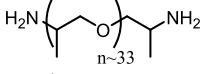
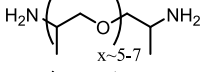
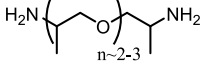
Three temperature ramps were performed (heating, cooling, and second heating) at a rate of 10 K · min⁻¹ under dry nitrogen flow. For the non-hermetic case, the temperature range was -90 to 200 °C. For the hermetic case, the upper temperature limit was set to slightly above the endset of the glass transition (first heating run) in order to erase the thermal history of the sample. In the second heating run, the maximum temperature was limited to 110 °C to prevent pressure build-up in the hermetic pan. The glass transition temperatures, T_g , were determined at the midpoint of the heat flow jump using the tangent method. The heat capacity jump at glass transition, ΔC_p , was determined from the net difference in heat flow normalized by sample mass at $T_g \pm 20 \text{ K}$, divided by the heating rate.

2.5. Dynamic mechanical analysis (DMA)

Specimens (10 x 30 x 0.3 mm³) were cut in the films for performing DMA analyses using an ARES G2 apparatus (TA Instruments). Experiments were performed in torsion mode at 1 Hz and dynamic strain amplitude between 0.15 % and 0.3 % in order to remain in the linear domain through the whole temperature range. The equipment was coupled to an air cooling system, providing dry air (0.1 % relative humidity) flowing through the chamber during the entire experiment to control the temperature in the range of -90 to 150 °C for each sample, with a heating rate of 3 K · min⁻¹.

The cooling step between the two heating runs was controlled (-10 K · min⁻¹) to avoid possible bending of the sample due to fast cooling. A small tensile axial force of approximately 5 gf ($\approx 0.05 \text{ N}$) was maintained throughout the measurement. The geometric factor, used to determine the shear modulus, was

Table 1: Prepolymer structures and corresponding molar masses (\overline{M}_n) from supplier datasheets.

Code	Formula	\overline{M}_n (g · mol ⁻¹)
DGEBA: LY 556		374
Jeffamine D2000		2,056
Jeffamine D400		460
Jeffamine D230		240

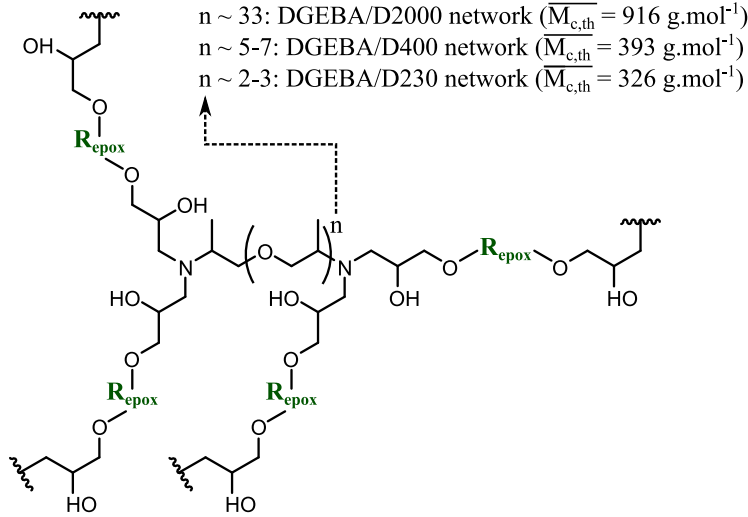


Figure 1: Schematic representation of the three networks (see Table 1 for the description of R_{epox}).

derived in accordance with the APN024 TA Instruments application note guidelines [36]. The Dirk Wötzel sample length correction was applied to account for clamping effects, that reduce the effective free length of the sample leading to artificial increase of modulus. This correction is applicable for a sample nominal length (l_{nom}) lying between 10 and 30 mm and the effective free length (l_{eff}) is obtained as follows:

$$l_{eff} = l_{nom} \left[1 - \kappa \frac{w}{l_{nom}} + 0.12886 \left(\frac{w}{l_{nom}} \right)^2 \right] \quad (2)$$

where a κ value of 0.65 was considered a suitable approximation for a Poisson's ratio of $\frac{1}{3}$ and a sample's aspect ratio $u > 10$ according to the APN024 note.

2.6. Broadband dielectric spectroscopy (BDS)

Dielectric spectroscopy measurements were performed using an Alpha-A impedance analyzer and Quatro apparatus (Novo-control) with a liquid nitrogen cooling system. Two consecutive measurements were performed within the temperature range of

-150 to 150 °C, with a 2 K increment between two isothermal data acquisition over a frequency range from 1 MHz to 40 mHz (with 3.0 V root mean square voltage amplitude, 9 points acquired per decade). Samples with a diameter of 30 mm were obtained from the 300 μ m tick films. They were gold-plated (with a diameter of 27 mm under secondary vacuum), then placed between two cylindrical brass disks of 20 mm diameter. A spring was used in the clamping step to compensate for sample contraction during cooling which could lead to imperfect contacts within the capacitor cell.

The sample current is converted into a voltage signal, which is compared to the generated (applied) voltage in the frequency domain using Fourier correlation analysis. This process allows for the determination of the sample's complex dielectric permittivity, $\epsilon^*(\omega) = \epsilon'(\omega) - i\epsilon''(\omega)$, where $\omega = 2\pi f$ is the angular frequency of the applied voltage.

The BDS spectra were fitted with the parametric Cole-Cole

equation:

$$\varepsilon^*(\omega) = \varepsilon_\infty + \frac{\varepsilon_s - \varepsilon_\infty}{1 + (i\omega\tau)^\alpha} \quad (3)$$

where α ($0 < \alpha \leq 1$) account for the width of the dispersion, ε_∞ and ε_s represent the high and low-frequency limits of the real part of the dielectric permittivity and the difference ($\varepsilon_s - \varepsilon_\infty$) is the relaxation strength, $\Delta\varepsilon$.

To overcome the possible masking of phenomena at low frequencies and high temperatures due to significant conduction contribution, a ‘‘conduction-free’’ approach of the imaginary part of the dielectric permittivity [37], was considered to obtain the relaxation times for the α -mode of the DGEBA/D230 and DGEBA/D400 networks. This approach is based on the logarithmic derivative:

$$\varepsilon''_{\text{deriv}} = -\frac{\pi}{2} \frac{\partial \varepsilon'(\omega)}{\partial \ln(\omega)} \approx \varepsilon'' \quad (4)$$

where ε' and ε'' are the real and imaginary components of dielectric permittivity, respectively.

3. Results and discussion

3.1. Thermal events

DSC thermograms of the three networks are presented in Figure 2. During the first heating runs, a water desorption endotherm was observed for all networks when using non-hermetic pans. For the DGEBA/D400 network, this desorption was preceded by a significant T_g overshoot corresponding to the enthalpy recovery associated with physical ageing, occurring at temperatures lower but close to T_g . The DGEBA/D230 network exhibited an additional small heat capacity jump prior to the main one, which will be discussed in conjunction with the delocalized molecular mobility modes.

The observed water desorption endotherm was expected since amine-based polyepoxy networks are able to absorb water under ambient storage conditions. Gravimetric measurements were conducted to assess the networks’ water uptake at equilibrium under ambient conditions. The results are summarized in Table 2. Taking into consideration the uncertainty of the gravimetric measurements, all networks exhibited similar equilibrium water uptake, suggesting a limited impact of crosslink density on equilibrium water uptake under relative humidity (not immersion) conditions. These results were consistent with the work of Linde *et al.* [33], who reported similar water uptake (around 3%) at 65 °C and 100% relative humidity for DGEBA/D230, DGEBA/D400, and DGEBA/D400/D2000 networks.

Table 2: Water uptake gravimetric measurements at equilibrium under ambient conditions for the three networks studied.

Network	Water uptake at equilibrium (wt%)
DGEBA/D2000	0.98 ± 0.20
DGEBA/D400	1.05 ± 0.20
DGEBA/D230	0.95 ± 0.20

During the second heating runs, water desorption endotherms were no longer observed and the enthalpy recovery endotherm was significantly reduced, allowing the determination of the heat capacity jump (ΔC_p) and glass transition temperatures for the *dry* networks, depicted in Figure 2.

The T_g and ΔC_p of the networks containing absorbed water in equilibrium with ambient conditions, *water-containing* networks, were determined during the second heating run using hermetic pans. First heating run allowed to erase physical ageing and the water desorption in the hermetic pans was considered negligible. These traces are depicted in Figure 2 as well.

In all the networks, the presence of water had negligible impact on ΔC_p (a decrease in ΔC_p with increasing crosslink density was observed for the *dry* networks). However, it significantly reduced the T_g in the DGEBA/D230 and DGEBA/D400 networks, by 11 K and 10 K respectively (hermetic pans), compared to the *dry* networks. Such level of T_g depression is commonly observed in epoxy networks containing absorbed water [32, 33]. This could be attributed to the weakening of intramolecular interactions formed between polar groups, known to strengthen the network, by the formation of hydrogen bonds between these groups and water molecules [38].

Conversely, for the DGEBA/D2000 network, no difference of T_g was observed between the *dry* and the *water-containing* samples, indicating negligible plasticizing effect in this network. This behavior might be associated with the polar sites within the crosslinks being kept distant by the long polypropylene glycol (PPG) chains of the D2000 hardener, thus impeding inter-crosslink physical interactions.

3.2. Dynamic mechanical and dielectric measurements

The effect of increasing crosslink density and water-polymer interactions on molecular dynamics was studied by dynamic mechanical analysis (DMA). The storage (G') and loss (G'') shear moduli for the two consecutive heating runs are depicted in Figure 3.

The samples were cured under mechanical constraint (between two metal plates), then cooled to room temperature still constrained, that is below T_g for DGEBA/D230 and DGEBA/D400. As a result, these internal stresses were released at the glass transition during the first DMA run, leading to lengthwise contraction (sample length variation reported as supplementary information, Figure S1). G' and G'' values were therefore corrected with the new sample cross-section, starting from T_α for the first run, and for the whole second run (DGEBA/D230 and DGEBA/D400).

The experimental average masses between crosslinks ($\overline{M_c}$) of the *dry* networks were calculated according to rubber elasticity theory as follows:

$$\overline{M_c} = \frac{\rho RT}{G'_R} \quad (5)$$

where G'_R is the storage modulus in the rubbery state, ρ is the network density at the temperature T (extrapolated from values at 25 °C taken from [39]), and R is the gas constant. The G'_R was taken at the minimum of G' in the rubbery region to exclude contributions of entropic elasticity.

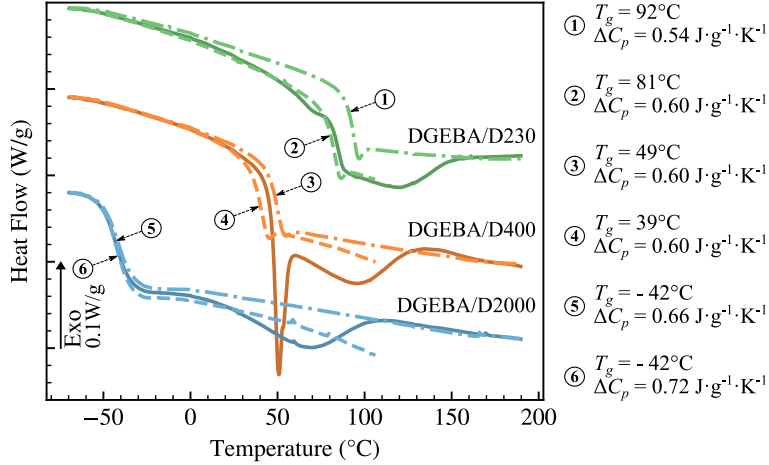


Figure 2: Differential scanning calorimetry traces for the three networks including first (—) and second (— · —) heating runs ($10 \text{ K}\cdot\text{min}^{-1}$) in non-hermetic pans and second heating runs in hermetic pans (— · —).

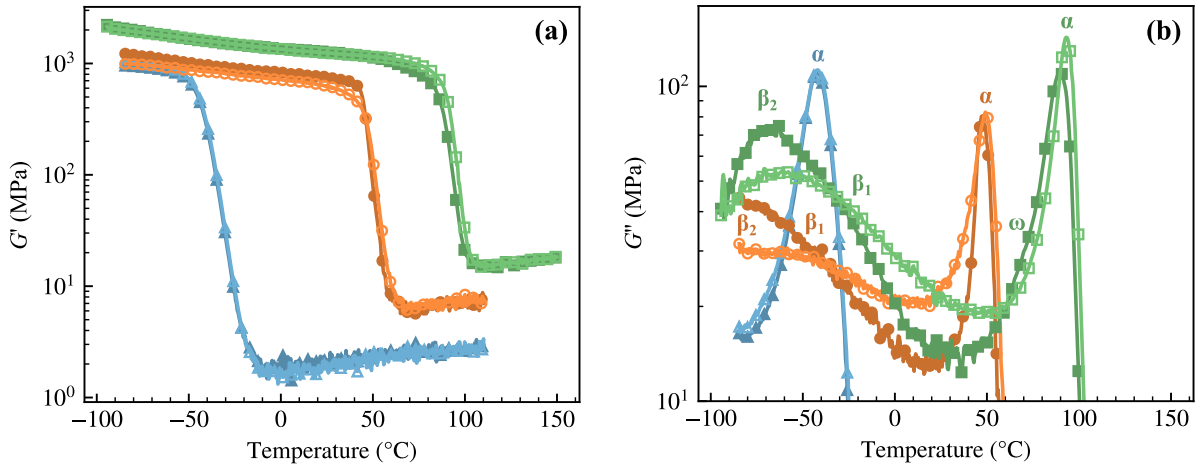


Figure 3: Dynamic storage (a) and loss (b) mechanical modulus of the three epoxy networks, as a function of temperature at 1 Hz, recorded during first (solid symbols) and second (open symbols) DMA ramps ($3 \text{ K}\cdot\text{min}^{-1}$): \blacktriangle DGEBA/D2000; \bullet DGEBA/D400; \blacksquare DGEBA/D230.

The theoretical ($\overline{M_{c,th}}$) values obtained using the method developed by Bell [35] (calculated with Equation 1) and the obtained experimental values ($\overline{M_{c,exp}}$) are given in Table 3.

Table 3: Storage modulus at the rubbery plateau G'_R , theoretical ($\overline{M_{c,th}}$) and experimental ($\overline{M_{c,exp}}$) average masses between crosslinks for the three networks.

Network	G'_R (MPa)	$\overline{M_{c,th}}$ ($\text{g}\cdot\text{mol}^{-1}$)	$\overline{M_{c,exp}}$ ($\text{g}\cdot\text{mol}^{-1}$)
DGEBA/D2000	2	916	1453
DGEBA/D400	6	393	502
DGEBA/D230	15	326	239

The increase of the modulus in the rubbery state with decreasing $\overline{M_c}$ (both theoretical and experimental), *i.e.* with decreasing PPG chain length of the diamine comonomer, was observed (Figure 3 and Table 3). The presence of network defects, such as single loop defects (particularly with the longer amine prepolymers [39]), but also the high sensitivity of $\overline{M_{c,exp}}$ to G'_R

from DMA measurements, may account for the discrepancy between theoretical and experimental values of $\overline{M_c}$. However, both trends are consistent with an increasing crosslink density in the three networks.

Broadband dielectric spectroscopy (BDS) measurements (two consecutive runs) were performed on the three networks. The samples were considered *dry* during the second heating run. The real, ϵ' , and imaginary, ϵ'' , parts of the dielectric permittivity at 1 Hz are presented separately for the three networks in Figure 4. The molecular relaxation modes of the *dry* and *water-containing* networks were investigated in detail. They will be described in the next section.

3.3. Influence of crosslink density and moisture on molecular dynamics

Four main molecular mobility modes were observed by BDS (Figure 4) across all the studied networks ($\gamma, \beta_2, \beta_1, \alpha$), followed by the charge transport process at high temperatures (σ). Some additional modes were observed separately: the ω -mode

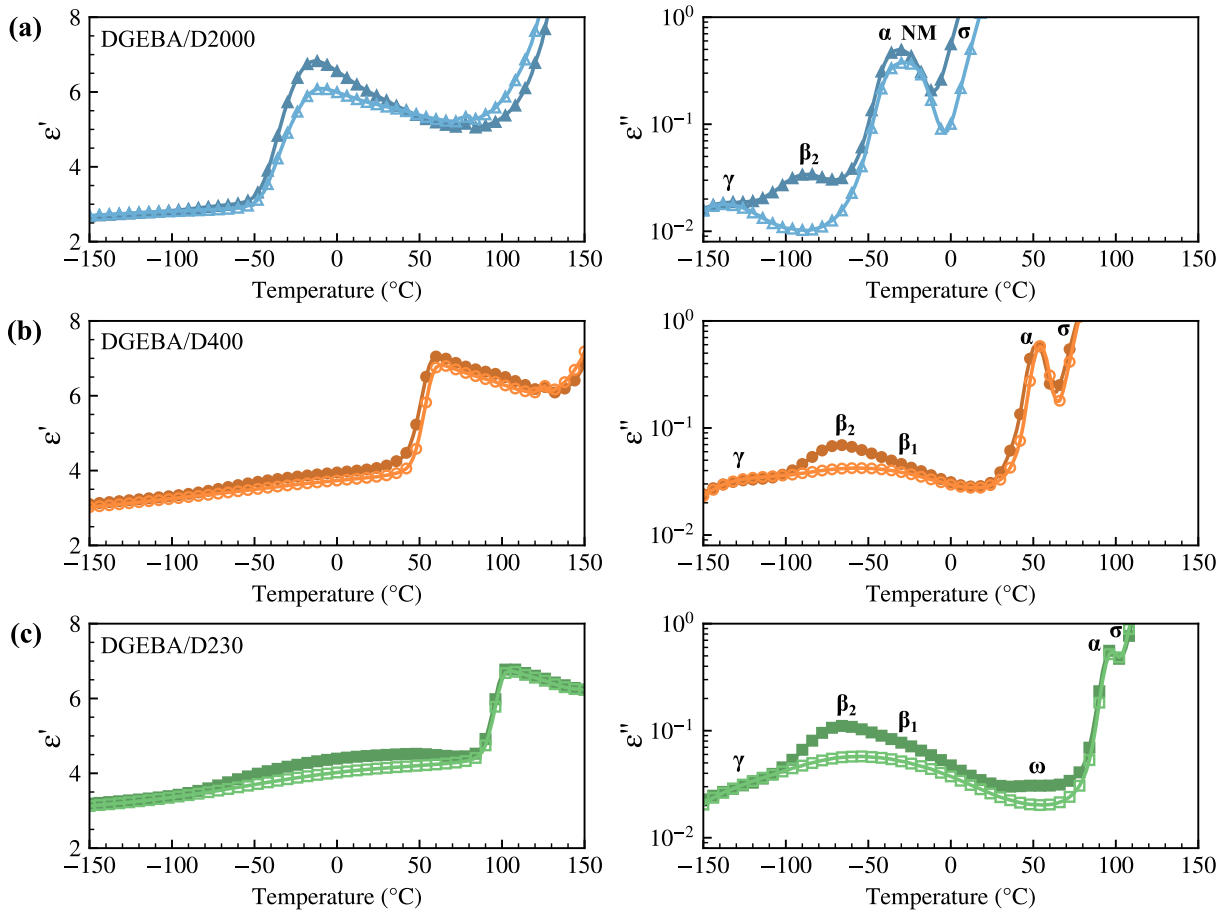


Figure 4: Real (left) and imaginary (right) parts of dielectric permittivity as a function of temperature for the three networks under the consecutive first (solid symbols) and second (open symbols) BDS runs at 1Hz: (a) \blacktriangle DGEBA/D2000; (b) \bullet DGEBA/D400; (c) \blacksquare DGEBA/D230.

in the DGEBA/D230 network (Figure 4 c) and the normal mode (NM) in the DGEBA/D2000 network (high temperature side of bimodal α relaxation, Figure 4 a). The ϵ'' relaxation map of the DGEBA/D400 network during the first heating run in BDS analysis is presented in Figure 5. The maps of the other networks (first and second runs) are provided as supplementary information (Figure S2).

A broad γ -mode was observed in the -150 to -50 °C temperature range for the DGEBA/D400 network, followed by an intense and bimodal β -mode, observed in the -100 to 10 °C temperature range, where the low-temperature side is called β_2 and the high-temperature side is called β_1 . From 50 to 90 °C, the main structural relaxation, α -mode, is observed, followed by conduction phenomena at high temperatures and low frequencies. The temperature dependence of each mode was investigated by determining the average relaxation time of the dipole distribution, τ , obtained by fitting the isothermal spectra with the empirical Cole-Cole equation Equation 3. The relaxation times obtained for the two BDS heating runs are summarized in the Arrhenius diagram in Figure 6.

The temperature dependences of the localized modes

$(\gamma, \beta_2, \beta_1)$ were evaluated according to the Arrhenius equation:

$$\tau_{\text{Arr}}(T) = \tau_0 e^{\frac{E_a}{RT}} \quad (6)$$

where τ_0 is the pre-exponential factor, E_a the activation energy, R the gas constant, and T the temperature.

The delocalized modes (α , NM) were evaluated using a form of the Vogel-Fulcher-Tammann (VFT) equation [40] based on the free volume interpretation of the glass transition by Cohen and Turnbull [41, 42], first described by Doolittle [43]:

$$\tau_{\text{VFT}}(T) = \tau_0 e^{\frac{1}{\alpha_f(T-T_\infty)}} \quad (7)$$

where τ_0 is the pre-exponential factor, α_f is the thermal expansion coefficient of the free volume and T_∞ is the Vogel's temperature.

In the following subsections, the influence of crosslink density and water sorption on the molecular mobility will be analyzed. We first present the delocalized mobility (associated with the glass transition), then we focus on secondary relaxation (glassy state).

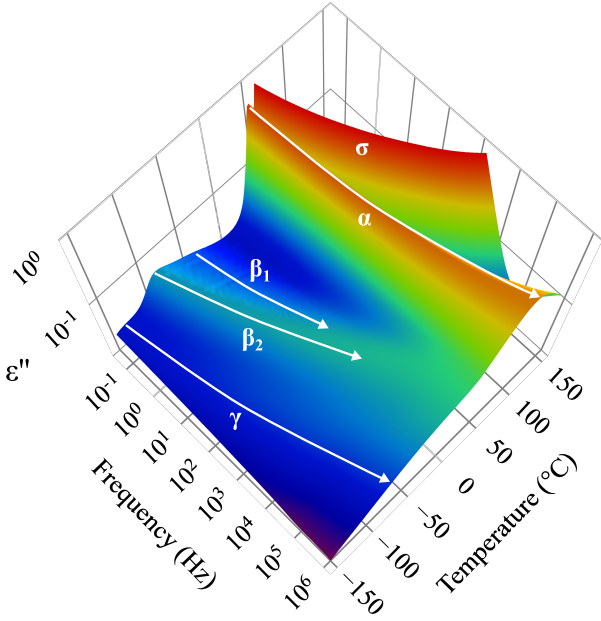


Figure 5: Relaxation map of the frequency and temperature dependences of ε'' for the DGEBA/D400 network during the first BDS run.

3.3.1. Delocalized molecular dynamics

The main structural relaxation, α -mode, which is related to glass transition, is observed as the dominant relaxation process in both DMA and BDS measurements.

By comparing the mode between the first (*water-containing*) and second (*dry*) DMA ramps (Figure 3), it was found that absorbed water induced a decrease in T_α of about 2 and 3 K for the DGEBA/D230 and DGEBA/D400 networks, respectively, while no difference was observed for the DGEBA/D2000 network. This result aligned with the T_g decrease observed by DSC, albeit to a lesser extent, which can be related to water desorption during the DMA experiment. Similar or even greater desorption during BDS measurements probably occurred due to longer experiment duration. Therefore, the assessment of water-induced effects on the α -mode through BDS and DMA measurements was limited in this case.

The relaxation times for the α -mode in the densely cross-linked networks, DGEBA/D230 and DGEBA/D400, were obtained by fitting a single Cole-Cole function to the ε^* data, employing the conduction-free approximation for ε'' as outlined in Equation 4. The α -mode observed by BDS for the DGEBA/D2000 network partially overlapped with the slower normal mode, NM, resulting in a bimodal appearance. The deconvolution of these two modes was performed using two Cole-Cole functions. The VFT fit parameters obtained for the α -mode, recorded during the second BDS run, for the three networks are reported as supplementary information (Table S1).

The normal mode was commonly observed in polymers having dipole moment component parallel to the chain backbone [44], such as PPGs [45, 46], therefore, in the DGEBA/D2000 network it was associated with the dipole inverted PPG backbone of the D2000 reacted at both ends [47]. The NM required the α -mobility of the network to operate. As a consequence, it

occurred at higher temperature.

During the first run only, the DGEBA/D230 network displayed an additional relaxation between α and β modes often referred to as ω -relaxation. It was observable in dielectric measurements close to 50 °C at 1 Hz (Figure 4 c) and in mechanical measurements, manifesting as a shoulder on the low temperature side of the α -mode (Figure 3 b). This relaxation could potentially be associated with the small heat capacity jump prior to the glass transition observed in the first DSC heating run, close to 65 °C (Figure 2). As short-range motions do not lead to C_p variations, the hypothetical correlation between this ΔC_p change and the ω -mode would be consistent with the presumed delocalized nature of the mode, commonly associated with regions presenting lower crosslink density in the network [23, 25].

3.3.2. Localized dynamics

The γ and β relaxation modes were present in all three networks during first BDS runs (Figure 4). The isofrequency (0.15 Hz) ε'' data in the region of the secondary modes (γ , β_1 and β_2) are displayed in Figure 7.

During the first run, strong overlapping of the γ and β modes occurred in all networks. This overlap persisted during the second run, but the amplitude of the β -peaks, particularly β_2 , decreased significantly. The intense β_2 mode in the first run masked the β_1 peak in isothermal data, complicating the deconvolution of these two contributions using Cole-Cole functions. To address this, the two β modes were deconvoluted in ε'' isofrequency data using two Gaussians. The first run γ and β_2 modes were also fitted together using two Cole-Cole functions in order to compare with the relaxation times found for β_2 using the Gaussian's approach. Examples of both fit methodologies are provided in supplementary information (Figure S3). During the second run, the β_1 relaxation times were obtained by adjusting one Gaussian to the ε'' isofrequency data for the DGEBA/D230 and DGEBA/D400 networks.

The isofrequency treatment using Gaussian functions yields the peak's maximum temperature position, T_{\max} , which can be related to the equivalent relaxation time by $\tau = \frac{1}{2\pi f}$, f being the corresponding frequency, under the assumption of symmetric τ spectral dispersion (*e.g.*, Debye or Cole-Cole type relaxations). This unusual method can introduce uncertainties in τ determination when deconvoluting overlapping modes, as is the case for β_1 and β_2 . In the present case, Figure 9 shows a constant 40% relative difference between the β_2 relaxation times obtained by this method and those from the combined Cole-Cole fit of β_2 and γ , resulting in the same β_2 activation energy for both methods. We ascribe this small discrepancy in relaxation times to the influence of β_1 , not considered in the Cole-Cole fits.

The second run γ -mode was fitted with a single Cole-Cole function for the DGEBA/D2000 and DGEBA/D400 networks. For the DGEBA/D230 network, the significant β -mode contribution across all isotherms prevented a reliable determination of the γ relaxation times.

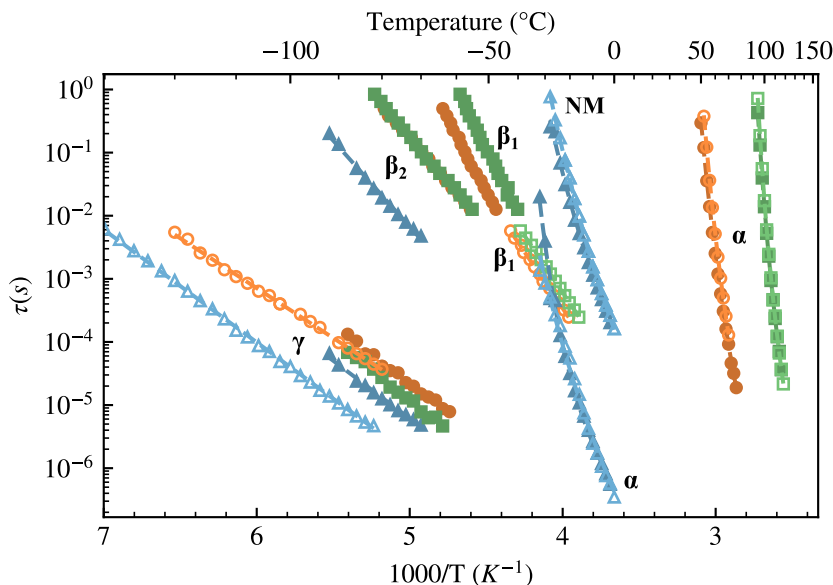


Figure 6: Arrhenius diagram of molecular relaxation modes of the three networks for the first (solid symbols) and second (open symbols) BDS runs: ▲ DGEBA/D2000; ● DGEBA/D400 ; ■ DGEBA/D230 ; - - - Arrhenius and VFT fits.

γ -mode

The γ -mode occurred in similar regions of the Arrhenius diagram (Figure 6) for the three networks studied during the first run and they displayed comparable activation energies of approximately $35 \text{ kJ} \cdot \text{mol}^{-1}$ (Table 4).

The γ -relaxation has been predominantly ascribed to the motion of polymethylene sequences of at least four carbon atoms in the diamine backbone [3, 5]. All the DGEBA/Jeffamine networks studied here lacked the referred minimal length of polymethylene sequence required to produce the mode, but contained methylenes interspersed by ether oxygen atoms in the PPG backbone of the diamine comonomer, believed to rotate in a way similar to polymethylene sequences. Indeed, polypropylene glycols exhibit a characteristic γ -relaxation, which has similar relaxation times [45, 46, 48, 49], and close activation energy ($E_a \approx 30 \text{ kJ} \cdot \text{mol}^{-1}$ [45, 46, 50]), as the γ -relaxations we observed. This similarity, already mentioned in the literature for the DGEBA/D2000 network [47], strongly suggested that the underlying molecular motions causing the γ -mode in PPGs are likely the same ones responsible for the mode observed in the networks.

For the DGEBA/D400 and DGEBA/D2000 networks, water desorption between the two BDS runs had no significant influence on the activation energy and relaxation strength of the γ -mode (Table 4). The minimal impact of water desorption observed here was consistent with previous findings regarding PPGs γ -mode before and after annealing [45, 46].

The weaker ΔE_γ observed for the DGEBA/D2000 network, compared to the more densely crosslinked networks, *i.e.* with shorter Jeffamine's PPG backbones, aligned with the previously reported decrease in ΔE_γ with increasing molecular weight in PPGs [51].

β -modes

The bimodal character of the β -mode was observed by both DMA and BDS during the first heating runs, particularly evident in the densely crosslinked networks (Figures 7 a and 3 b), DGEBA/D230 and DGEBA/D400, but also present in the DGEBA/D2000 network (Figure 7 b). This bimodality indicated two populations of relaxing units, here called β_2 (at low temperature) and β_1 (at high temperature).

The evolution of the β loss peaks during both BDS heating runs with respect to frequency and temperature through the multiple isofrequency and the isothermal curves is depicted for the DGEBA/D230 network in Figure 8, which evidenced the impossibility to separate β_2 and β_1 in the spectra (Figure 8 b and d). The relaxation times of β_1 and β_2 modes are represented in the Arrhenius diagram in Figure 9 and the corresponding activation energies are depicted in Table 4.

During the second run, the bimodal character was no longer evident (3D relaxation maps Figure S2 d and f for instance), suggesting that the two contributions were affected differently by the presence of water in the network. However, at low frequencies (Figure 7), there were still signs of residual β_2 in the second BDS runs. The amplitude decrease after water desorption was noticeably more pronounced in the low-temperature side of the mode, β_2 , suggesting the existence of a motional process associated with water-polymer interactions.

The localized motions of hydroxyether groups have been considered to be the primary molecular origin of the β -relaxation in epoxy-amine networks [3–5, 10]. Numerous sorption studies reported an increase in the β -mode amplitude upon water absorption, attributed to the formation of hydrogen bonds between water molecules and the hydroxyl groups from hydroxyether units [20, 24, 26, 34, 52]. The active participation of water molecules in the relaxation process has been proposed

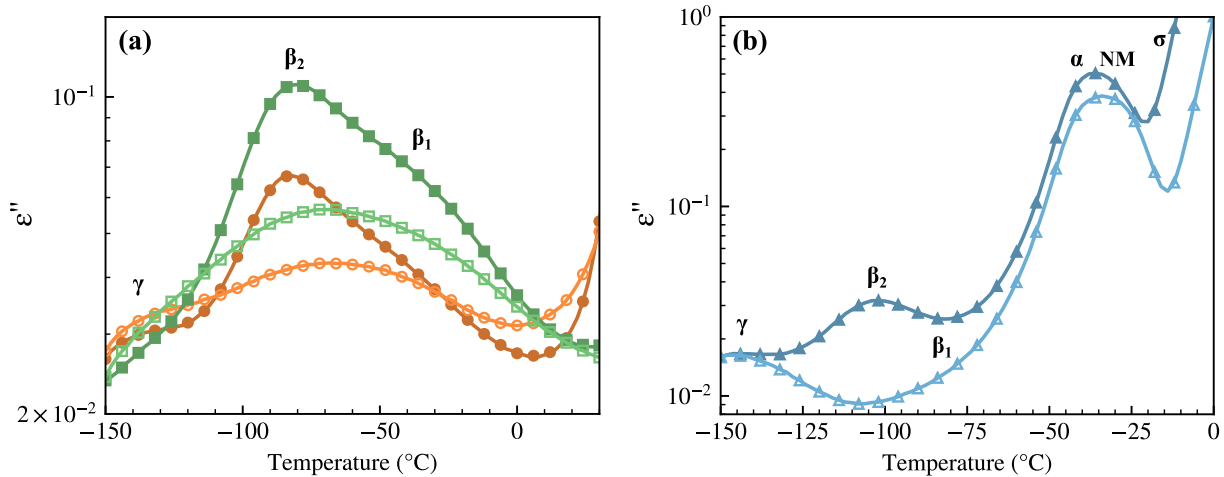


Figure 7: Imaginary part of the dielectric permittivity as a function of temperature at 0.15 Hz under the consecutive first (solid symbols) and second (open symbols) BDS runs: (a) \bullet DGEBA/D400; \blacksquare DGEBA/D230, and (b) \blacktriangle DGEBA/D2000.

Table 4: Arrhenius parameters of the γ , β_1 and β_2 modes and mean relaxation strength, $\Delta\epsilon$, of the γ -mode from BDS measurements.

Network	Heating run	γ			β_1		β_2	
		τ_0 (s)	E_a (kJ \cdot mol $^{-1}$)	$\Delta\epsilon$	τ_0 (s)	E_a (kJ \cdot mol $^{-1}$)	τ_0 (s)	E_a (kJ \cdot mol $^{-1}$)
DGEBA/D2000	1	$4 \cdot 10^{-15}$	35	0.29	—	—	$2 \cdot 10^{-16}$	52
	2	$2 \cdot 10^{-15}$	34	0.22	—	—	—	—
DGEBA/D400	1	$2 \cdot 10^{-14}$	34	0.54	$5 \cdot 10^{-23}$	88	$2 \cdot 10^{-15}$	54
	2	$2 \cdot 10^{-13}$	30	0.48	$2 \cdot 10^{-18}$	69	—	—
DGEBA/D230	1	$2 \cdot 10^{-15}$	37	0.5	$1 \cdot 10^{-23}$	94	$1 \cdot 10^{-15}$	55
	2	—	—	—	$2 \cdot 10^{-18}$	69	—	—

[26, 52, 53], including the hypothesis that the water's dipole moment contributed to that of the network hydroxyl group [53]. Therefore, the β_2 -mode, observable in the presence of absorbed water, was attributed to hydroxyether units interacting with water molecules, while the β_1 -mode was ascribed to the motions of hydroxyether units not interacting with water.

We started by studying the manifestation of the β modes in the densely crosslinked networks, for which it was possible to obtain the relaxation times of both contributions. In Figure 9, the two Gaussian deconvolution of the isofrequency curves yielded nearly the same β_2 relaxation times as the two Cole-Cole fit with the γ mode, which validated the method for extracting τ .

The relaxation times of β_2 were shorter than those of β_1 (Figure 9), and the activation energies lower (Table 4), irrespective of the run, suggesting that the energy barrier to initiate hydroxyether mobility was reduced as a result of interaction with water molecules.

The area of the mechanical β loss peak was qualitatively the same in the two DMA runs (Figure 3b), the low-temperature part of the relaxation being exacerbated at the expense of its high-temperature part in the presence of water. This behavior was not observed in BDS, where absorbed water caused the area

to increase over the whole temperature range of the relaxation, particularly on the low-temperature side of the mode, β_2 . This could indicate either an increased density of relaxing units or an increased dipole moment contribution, with the comparison to mechanical relaxation favoring the latter possibility. The additional dipole moment contribution could result from the strong interaction between the network's hydroxyl groups and water molecules.

In the *water-containing* DGEBA/D400 and DGEBA/230 networks, the β_2 relaxation times were superimposed (Figure 9), indicating that the hydroxyether groups interacting with water molecules presented similar environments in both networks.

Regarding the β_1 -mode, the hydroxyether group rotation is believed to be hindered by the pendant hydroxyl group, capable of forming hydrogen bonds with each other [4]. With increasing crosslink density, there are greater possibilities for intramolecular hydrogen bonding, leading to physical environments with higher hindrance of the hydroxyether group rotation. This is consistent with the longer relaxation times of the β_1 -mode in DGEBA/D230 compared to DGEBA/D400 network, also presenting higher activation energy (about 7%).

The activation energies of the β_1 -mode also seemed to change for both networks across the consecutive runs, being

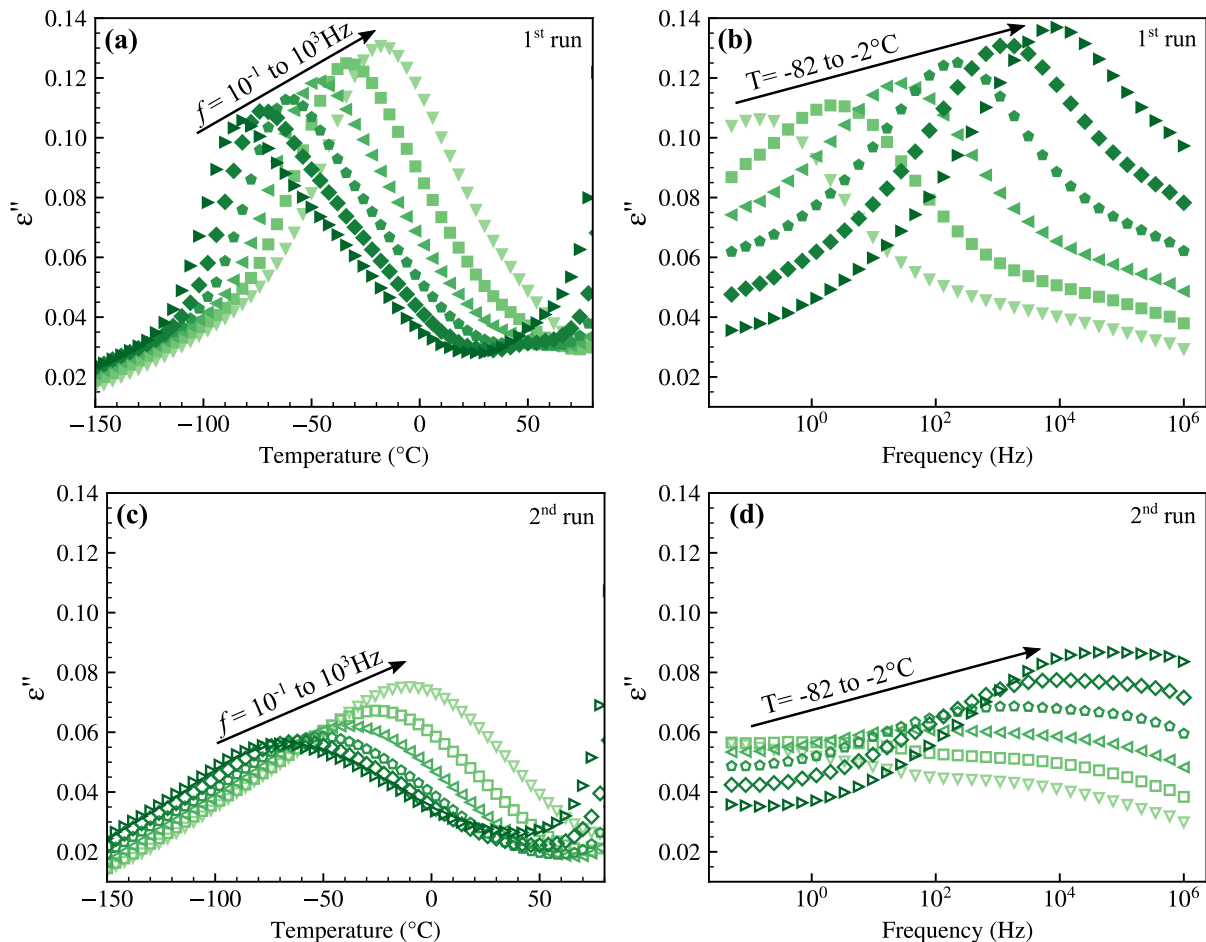


Figure 8: Isothermal and isofrequency ε'' curves of β -modes for the DGEBA/D230 network obtained by BDS; (a) (c) first run (solid symbols); (b) (d) second run (open symbols).

higher in the presence of water (Table 4). It is therefore possible that the distribution of physical environments of the hydroxyether groups is different between *dry* and *water-containing* networks, as τ and E_a of the β_1 -mode in the DGEBA/D230 network are higher compared to the DGEBA/D400 network during the first run. This difference could arise from the hydroxyether groups being, on average, more constrained by intramolecular interactions in the DGEBA/D230 network, once less hindered groups are preferentially interacting with water. However, this slight discrepancy regarding the β_1 -mode in the two consecutive runs could also be due to the contribution of a residual β_2 contribution in the second BDS run, unaccounted for in the single Gaussian fit of the broad relaxation observed on the isofrequency curves (Figure 7a), therefore slightly altering the β_1 relaxation times.

With the DGEBA/D2000 network, the α -mode fell within the range of β_1 -mode in the densely crosslinked networks (see Figure 6). A slight shoulder in the low-temperature side of the DGEBA/D2000 α -mode (Figure 7 b) could correspond to the β_1 -mode of DGEBA/D2000 network, that in this case, would occur practically simultaneously with the large-scale segmental motions and could be an initiator of the dynamic glass transition. Polypropylene glycols have been reported to dis-

play a β -relaxation process associated with the hydration of the PPG chain [45, 46]. The comparison of our data with this water-related process in PPGs revealed strong similarity of relaxation times with the β_2 -mode in the *water-containing* DGEBA/D2000 network, which was shifted towards lower temperatures by approximately 25 K (Figures 7 and 9) compared to the DGEBA/D230 and DGEBA/D400 networks, while presenting a similar activation energy of $52 \text{ kJ} \cdot \text{mol}^{-1}$ (Table 4). Such a contribution could also be convoluted in the β_2 temperature and frequency region studied here, with the hydroxyether-water interaction assignment developed for the densely crosslinked networks. The DGEBA/D2000 network, with the long PPG backbone from the D2000 hardener, displayed different behaviours in terms of water induced plasticization (no decrease in T_g), mechanical and dielectric relaxation (normal mode), which raises questions about the comparison with more densely crosslinked epoxy-amine networks. Perhaps it resembles the behaviour of linear PPG chains in some aspects, such as the β_2 origin and the unclear manifestation of β_1 -mode. Further investigation is needed to elucidate these particularities of the DGEBA/D2000 system, which is currently being studied by our group.

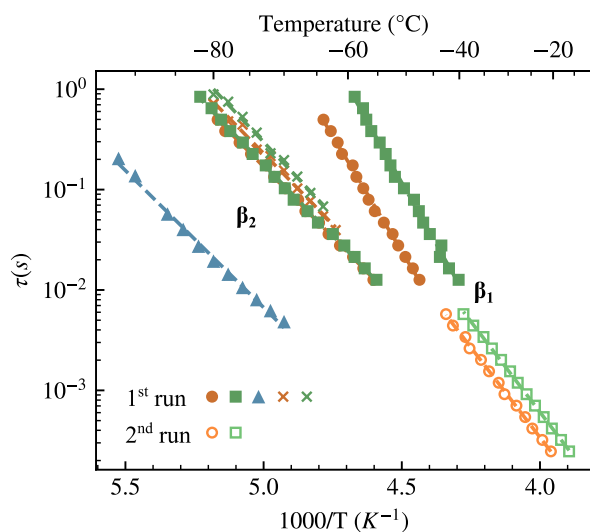


Figure 9: Arrhenius diagram of β -mode relaxation times obtained from BDS isofrequency and isotherm spectra fits of first (solid symbols) and second (open symbols) runs: ■ DGEBA/D230; ● DGEBA/D400 ; ▲ DGEBA/D2000. For DGEBA/D230 and DGEBA/D400, two Gaussians were used on the first run isofrequency curves, only one Gaussian on the second run. Crosses (x) correspond to Cole-Cole fits of β_2 and γ -modes (BDS spectra). For DGEBA/D2000, the β_2 spectra were fitted with the Cole-Cole equation.

4. Conclusion

The influence of ambient storage conditions, and consequently absorbed water, and crosslink density on the molecular mobility of epoxy-amine networks was studied through the analysis of two consecutive heating runs using DSC, DMA, and BDS on three epoxy-amine networks displaying increasing crosslink density.

Significant water-induced effects were observed on localized molecular mobility modes. The increase in dielectric β -relaxation amplitude with water absorption, commonly observed in epoxy-amine networks, and its bimodal nature were proposed to result from hydroxyether groups interacting with water molecules (β_2) and hydroxyethers interacting with each other (β_1). The former presented faster dynamics and lower activation energies in the densely crosslinked networks. When water was removed, a broad β_1 mode was observed, ascribed to a wide range of molecular environments of the hydroxyether groups, capable of engaging in intramolecular interactions that constrain the group rotation. The presence of a residual β_2 contribution in the second runs, at low frequencies, suggested the difficulty to achieve complete dryness in epoxy-amine networks.

With significantly longer PPG backbone, the DGEBA/D2000 may share properties with linear PPG chains, such as the water-related relaxation and normal mode.

This study highlighted the importance of controlling sample conditioning before measurements, especially in molecular mobility studies, to avoid potentially erroneous conclusions by overlooking water-induced effects on molecular mobility modes. Such dependence of secondary relaxations to small amounts of absorbed water are of importance in the applications

of epoxy networks (for instance, their mechanical properties at room temperature are strongly influenced by the β relaxations). Furthermore, it enabled the differentiation of changes in molecular mobility due to moisture content from those observed due to modifications in network crosslink density, which yielded insights for better understanding of the complex molecular mechanisms involved in secondary relaxations of epoxy-amine networks.

Declaration of competing interest

The authors declare that they have no known competing financial interests or personal relationships that could have appeared to influence the work reported in this paper.

Acknowledgements

The French Ministry of Education and Research is gratefully recognized for providing a grant for this project and the Ecole Doctorale Matériaux de Lyon ED034 for their financial support.

References

- [1] J.-F. Gérard, J. Galy, J.-P. Pascault, S. Cukierman, J.-L. Halary, Viscoelastic response of model epoxy networks in the glass transition region, *Polymer Engineering & Science* 31 (8) (1991) 615–621.
- [2] J.-L. Halary, S. Cukierman, L. Monnerie, Relations entre structure chimique et propriétés mécaniques dans les réseaux époxydes, *Bulletin des sociétés chimiques belges* 98 (9-10) (1989) 623–634.
- [3] J. M. Charlesworth, Effect of crosslink density on the molecular relaxations in diepoxide-diamine network polymers. part 1. the glassy region, *Polymer Engineering & Science* 28 (4) (1988) 221–229.
- [4] G. Pogany, Gamma relaxation in epoxy resins and related polymers, *Polymer* 11 (2) (1970) 66–78.
- [5] M. Ochi, M. Okazaki, M. Shimbo, Mechanical relaxation mechanism of epoxy resins cured with aliphatic diamines, *Journal of Polymer Science: Polymer Physics Edition* 20 (4) (1982) 689–699.
- [6] J. G. Williams, The beta relaxation in epoxy resin-based networks, *Journal of Applied Polymer Science* 23 (12) (1979) 3433–3444.
- [7] A. C. Grillet, J. Galy, J.-F. Gérard, J.-P. Pascault, Mechanical and viscoelastic properties of epoxy networks cured with aromatic diamines, *Polymer* 32 (10) (1991) 1885–1891.
- [8] S. Cukierman, J.-L. Halary, L. Monnerie, Dynamic mechanical response of model epoxy networks in the glassy state, *Polymer Engineering & Science* 31 (20) (1991) 1476–1482.
- [9] L. Heux, J.-L. Halary, F. Lauprêtre, L. Monnerie, Dynamic mechanical and ^{13}C nmr investigations of molecular motions involved in the β relaxation of epoxy networks based on DGEBA and aliphatic amines, *Polymer* 38 (8) (1997) 1767–1778.
- [10] F. Lauprêtre, R.-P. Eustache, L. Monnerie, High-resolution solid-state ^{13}C nuclear magnetic resonance investigation of local motions in model epoxy resins, *Polymer* 36 (2) (1995) 267–274.
- [11] E. Butta, A. Livi, G. Levita, P. Rolla, Dielectric analysis of an epoxy resin during cross-linking, *Journal of Polymer Science Part B: Polymer Physics* 33 (16) (1995) 2253–2261.
- [12] M. Chevalier, E. Dantras, C. Tonon, P. Guigue, C. Lacabanne, C. Puig, C. Durin, Correlation between sub- T_g relaxation processes and mechanical behavior for different hydrothermal ageing conditions in epoxy assemblies, *Journal of Applied Polymer Science* 115 (2) (2010) 1208–1214.
- [13] R. Delannoy, B. Quélenec, V. Tognetti, L. Delbreilh, N. Delpouve, E. Richaud, Glass and sub-glass relaxation changes induced by thermal ageing of epoxy-amine polymer networks—a dma study, *Polymer Degradation and Stability* 216 (2023) 110487.

- [14] Y.-g. Won, J. Galy, J.-F. Gérard, J.-P. Pascault, V. Bellenger, J. Verdu, Internal antiplasticization in copolymer and terpolymer networks based on diepoxides, diamines and monoamines, *Polymer* 31 (9) (1990) 1787–1792.
- [15] F. Dammont, T. Kwei, Dynamic mechanical properties of aromatic, aliphatic, and partially fluorinated epoxy resins, *Journal of Polymer Science Part A-2: Polymer Physics* 5 (4) (1967) 761–769.
- [16] T. Takahama, P. Geil, The β relaxation behavior of bisphenol-type resins, *Journal of Polymer Science: Polymer Physics Edition* 20 (11) (1982) 1979–1986.
- [17] E. Urbaczewski-Espuche, J. Galy, J.-F. Gérard, J.-P. Pascault, H. Sautereau, Influence of chain flexibility and crosslink density on mechanical properties of epoxy/amine networks, *Polymer Engineering & Science* 31 (22) (1991) 1572–1580.
- [18] V. A. Bershtein, N. N. Peschanskaya, J.-L. Halary, L. Monnerie, The sub- T_g relaxations in pure and antiplasticized model epoxy networks as studied by high resolution creep rate spectroscopy, *Polymer* 40 (24) (1999) 6687–6698.
- [19] O. Delatycki, J. C. Shaw, J. G. Williams, Viscoelastic properties of epoxy-diamine networks, *Journal of Polymer Science Part A-2: Polymer Physics* 7 (5) (1969) 753–762.
- [20] S. Pangrle, C. Wu, P. Geil, Low temperature relaxation of DGEBA epoxy resins: a thermally stimulated discharge current (TSDC) study, *Polymer Composites* 10 (3) (1989) 173–183.
- [21] P. N. Patil, S. K. Rath, S. K. Sharma, K. Sudarshan, P. Maheshwari, M. Patri, S. Praveen, P. Khandelwal, P. K. Pujari, Free volumes and structural relaxations in diglycidyl ether of bisphenol-a based epoxy-polyether amine networks, *Soft Matter* 9 (13) (2013) 3589–3599.
- [22] R. Ramsdale-Capper, J. P. Foreman, Internal antiplasticisation in highly crosslinked amine cured multifunctional epoxy resins, *Polymer* 146 (2018) 321–330.
- [23] R. G. C. Arridge, J. H. Speake, Mechanical relaxation studies of the cure of epoxy resins: 2. activation energy of the γ -process in amine-cured epoxy resins, *Polymer* 13 (9) (1972) 450–454.
- [24] D. Colombini, J. Martinez-Vega, G. Merle, Dynamic mechanical investigations of the effects of water sorption and physical ageing on an epoxy resin system, *Polymer* 43 (16) (2002) 4479–4485.
- [25] J. D. Keenan, J. C. Seferis, J. T. Quinlivan, Effects of moisture and stoichiometry on the dynamic mechanical properties of a high-performance structural epoxy, *Journal of Applied Polymer Science* 24 (12) (1979) 2375–2387.
- [26] C. Maggana, P. Pissis, TSDC studies of the effects of plasticizer and water on the sub- T_g relaxations of an epoxy resin system, *Journal of Macromolecular Science, Part B: Physics* 36 (6) (1997) 749–772.
- [27] P. Zinck, J.-F. Gérard, Polyepoxide–water interactions: Influence of the chemical structure of the network, *Polymer Degradation and Stability* 93 (6) (2008) 1231–1237.
- [28] T. Lefort, J. Duchet-Rumeau, S. Livi, D. Bachelier, S. Pruvost, Dielectric behaviour of an epoxy network cured with a phosphonium-based ionic liquid, *Polymer* 222 (2021) 123645.
- [29] J. Duchet, J.-P. Pascault, Do epoxy–amine networks become inhomogeneous at the nanometric scale?, *Journal of Polymer Science Part B: Polymer Physics* 41 (20) (2003) 2422–2432.
- [30] W. Mikols, J. Seferis, A. Apicella, L. Nicolais, Evaluation of structural changes in epoxy systems by moisture sorption-desorption and dynamic mechanical studies, *Polymer Composites* 3 (3) (1982) 118–124.
- [31] J. Mijović, H. Zhang, Local dynamics and molecular origin of polymer network- water interactions as studied by broadband dielectric relaxation spectroscopy, ftir, and molecular simulations, *Macromolecules* 36 (4) (2003) 1279–1288.
- [32] T. Ellis, F. Karasz, Interaction of epoxy resins with water: the depression of glass transition temperature, *Polymer* 25 (5) (1984) 664–669.
- [33] E. Linde, N. H. Giron, M. C. Celina, Water diffusion with temperature enabling predictions for sorption and transport behavior in thermoset materials, *Polymer* 153 (2018) 653–667.
- [34] R. A. Pethrick, E. A. Hollins, L. McEwan, A. Pollock, D. Hayward, P. Johncock, Effect of cure temperature on the structure and water absorption of epoxy/amine thermosets, *Polymer International* 39 (4) (1996) 275–288.
- [35] J. P. Bell, Structure of a typical amine-cured epoxy resin, *Journal of Polymer Science Part A-2: Polymer Physics* 8 (3) (1970) 417–436.
- [36] A. Franck, Evaluation of the correct modulus in rectangular torsion, TA-Instruments application note APN024 V2 1–6.
- [37] M. Wübbenhorst, J. Van Turnhout, Conduction-free dielectric loss $\frac{\partial \epsilon}{\partial \ln f}$ – a powerful tool for the analysis of strong, *Dielectrics Newsletter, NOVO-CONTROL, GmbH, Hundsangen* (2000) 1–8.
- [38] J. Zhou, J. P. Lucas, Hygrothermal effects of epoxy resin. part i: the nature of water in epoxy, *Polymer* 40 (20) (1999) 5505–5512.
- [39] I. M. McAninch, G. R. Palmese, J. L. Lenhart, J. J. La Scala, Characterization of epoxies cured with bimodal blends of polyetheramines, *Journal of Applied Polymer Science* 130 (3) (2013) 1621–1631.
- [40] C. Lacabanne, D. Chatain, Depolarization thermocurrents in amorphous polymers, *Journal of polymer science: polymer physics edition* 11 (12) (1973) 2315–2328.
- [41] M. H. Cohen, D. Turnbull, Molecular transport in liquids and glasses, *The Journal of Chemical Physics* 31 (5) (1959) 1164–1169.
- [42] J. Ferry, *Viscoelastic Properties of Polymers*, 3rd Edition, Wiley, 1980, pp. 280-289.
- [43] A. K. Doolittle, Studies in Newtonian Flow. II. The Dependence of the Viscosity of Liquids on Free-Space, *Journal of Applied Physics* 22 (12) (1951) 1471.
- [44] H. Watanabe, Dielectric relaxation of type-a polymers in melts and solutions, *Macromolecular rapid communications* 22 (3) (2001) 127–175.
- [45] K. Kaminski, W. Kipnusu, K. Adrjanowicz, E. Mapesa, C. Iacob, M. Jasurkowska, P. Włodarczyk, K. Grzybowska, M. Paluch, F. Kremer, Comparative study on the molecular dynamics of a series of polypropylene glycols, *Macromolecules* 46 (5) (2013) 1973–1980.
- [46] C. Gainaru, W. Hiller, R. Bohmer, A dielectric study of oligo-and poly (propylene glycol), *Macromolecules* 43 (4) (2010) 1907–1914.
- [47] T. Kourkoutsaki, E. Logakis, I. Kroutilova, L. Matejka, J. Nedbal, P. Pissis, Polymer dynamics in rubbery epoxy networks/polyhedral oligomeric silsesquioxanes nanocomposites, *Journal of Applied Polymer Science* 113 (4) (2009) 2569–2582.
- [48] K. Ngai, S. Pawlus, K. Grzybowska, K. Kaminski, S. Capaccioli, M. Paluch, Does the johari–goldstein β -relaxation exist in polypropylene glycols?, *Macromolecules* 48 (12) (2015) 4151–4157.
- [49] K. Grzybowska, S. Pawlus, M. Mierzwa, M. Paluch, K. Ngai, Changes of relaxation dynamics of a hydrogen-bonded glass former after removal of the hydrogen bonds, *The Journal of chemical physics* 125 (14) (2006).
- [50] H. Omar, G. J. Smales, S. Henning, Z. Li, D.-Y. Wang, A. Schönhals, P. Szymoniak, Calorimetric and dielectric investigations of epoxy-based nanocomposites with halloysite nanotubes as nanofillers, *Polymers* 13 (10) (2021) 1634.
- [51] K. Grzybowska, A. Grzybowski, J. Ziolo, S. Rzoska, M. Paluch, Anomalous behavior of secondary dielectric relaxation in polypropylene glycols, *Journal of Physics: Condensed Matter* 19 (37) (2007) 376105.
- [52] A. Roggero, N. Caussé, N. Pèbère, E. Dantzas, VFT to Arrhenius crossover at the dynamic glass transition of an epoxy network as revealed by dielectric experiments in continuous immersion, *Polymer* 241 (2022) 124542.
- [53] J. Mijović, H. Zhang, Molecular dynamics simulation study of motions and interactions of water in a polymer network, *The Journal of Physical Chemistry B* 108 (8) (2004) 2557–2563.

Supplementary information

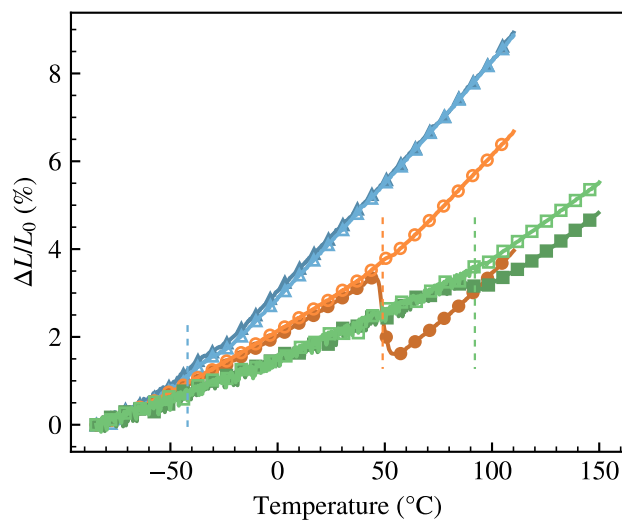


Figure S1: Sample length change (ΔL) normalized by initial length (L_0) as a function of temperature obtained by DMA under the consecutive first (solid symbols) and second (open symbols) runs ($3 \text{ K} \cdot \text{min}^{-1}$); \blacktriangle —DGEBA/D2000 \bullet —DGEBA/D400 ; \blacksquare —DGEBA/D230. Dashed vertical lines indicate the calorimetric T_g (second run) for the networks DGEBA/D2000, DGEBA/D400 and DGEBA/D230 in increasing temperature order.

Table S1: VFT fit parameters (second BDS run): pre-exponential factor (τ_0); free volume expansion coefficient (α_f); Vogel temperature (T_∞) associated with the α -mode of the three networks.

Mode-Network	τ_0 (s)	α_f (K^{-1})	T_∞ ($^\circ\text{C}$)
α -DGEBA/D2000	$5 \cdot 10^{-11}$	$2 \cdot 10^{-3}$	-56
α -DGEBA/D400	$3 \cdot 10^{-12}$	$1 \cdot 10^{-3}$	13
α -DGEBA/D230	$6 \cdot 10^{-12}$	$1 \cdot 10^{-3}$	59

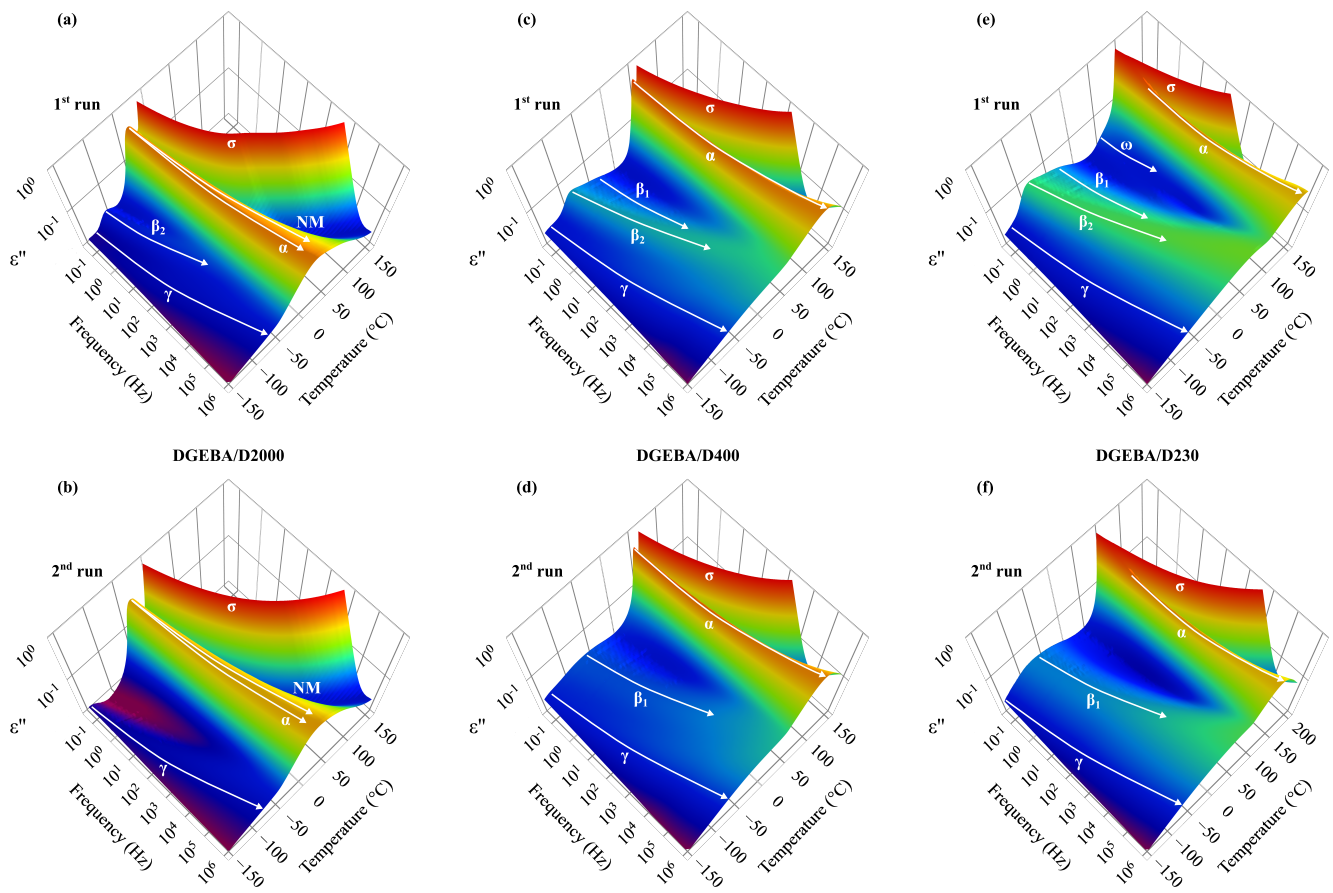


Figure S2: 3D relaxation maps from two consecutive BDS runs performed on the three networks.

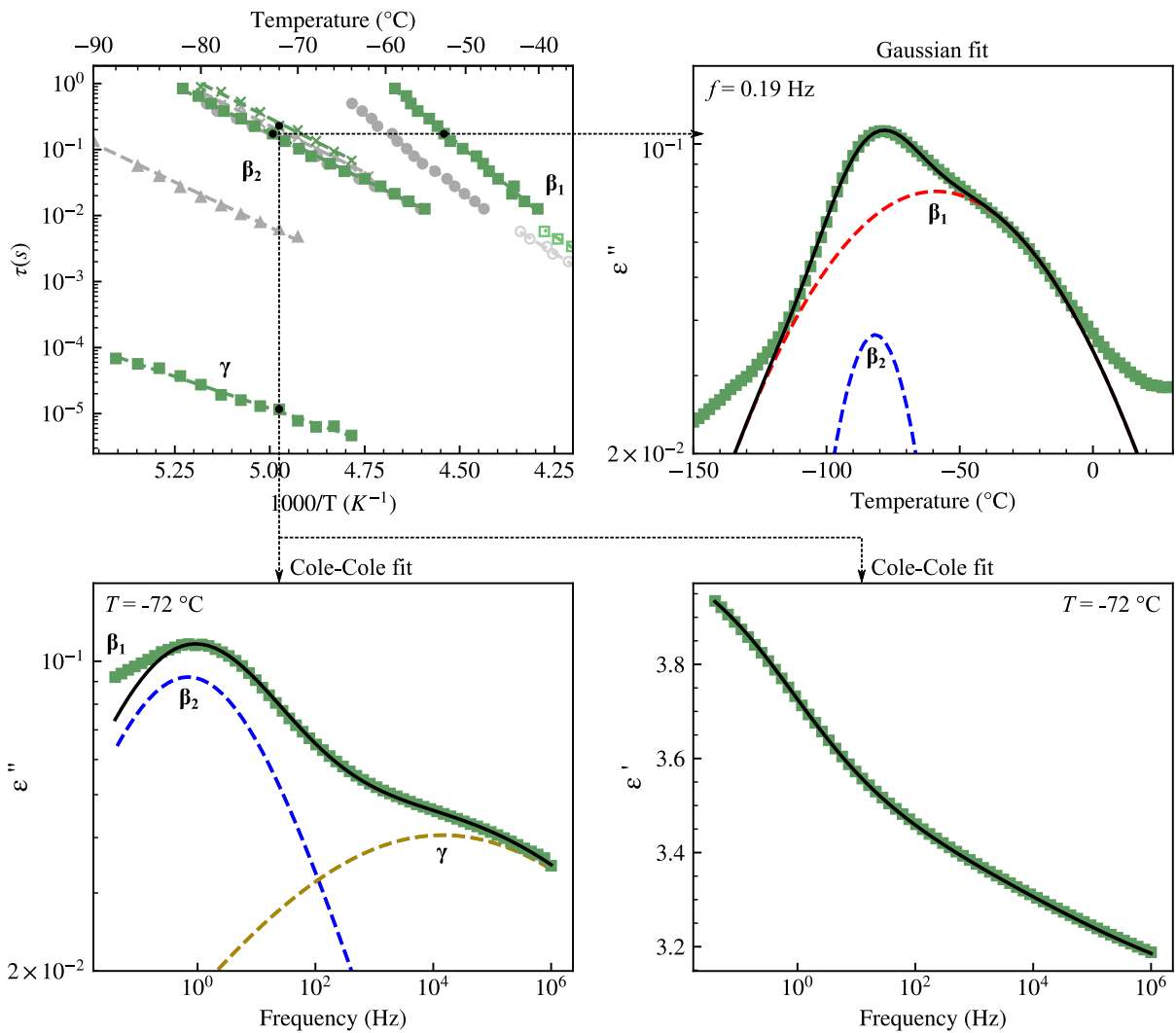


Figure S3: Arrhenius diagram (top-left) highlighting the delocalized modes of the DGEBA/D230 network during the first run, with other modes depicted in grayscale. Symbols correspond to those in Figure 9. Examples of isofrequency fit (top-right) for the β_1 and β_2 modes using two Gaussian functions and isothermal fit (ϵ'' : bottom-left and ϵ' : bottom-right) for the γ and β_2 modes using two Cole-Cole functions are correlated with their respective points in the Arrhenius diagram. The dashed lines (---) represent individual Gaussian or Cole-Cole fitted functions for each mode, while the solid line (—) represents the final fit, which is the sum of the two individual functions.